Apolipoprotein(a) Binds to Low-Density Lipoprotein at Two Distant Sites in Lipoprotein(a)†

Shaohua Xu*

Department of Medicine, The University of Chicago, Chicago, Illinois 60637

Received December 3, 1997; Revised Manuscript Received March 11, 1998

ABSTRACT: Lipoprotein(a) [Lp(a)] consists of low-density lipoprotein (LDL) and apolipoprotein(a) [apo(a)] linked with a disulfide bond. Scanning force microscopy (SFM) of Lp(a) showed, for the first time, a belt-like structure of apo(a) with both ends attached to a spherical LDL. The two ends of apo(a) were bound to the LDL sphere at two distant sites. Occasionally, the ends were attached to two touching spheres. Under the same imaging conditions, LDL appeared as individual spheres. Electron microscopy (EM) studies of Lp(a) by several groups over the past decade failed to reveal this belt-like structure of apo(a). Images of isolated apo(a) in air or in phosphate buffer showed apo(a) as individual belts, and these belts tended to crowd together. Lp(a) formed leaf-like aggregates; apo(a) aggregates were fishnet-like, whereas LDL aggregates were less characteristic. Quantitative analysis of Lp(a) showed the diameter of the LDL to be 24.8 ± 8.7 nm ($n = 46$), which is close to the reported value of 24.2 ± 4.2 nm found with EM. The length of the belts attached to the spheres was measured to be 173.5 ± 6.6 nm ($n = 15$). I also found, by using a functionalized tip, that the interaction force between apo(a) and its ligand, lysine, was related to the ionic strength of the bulk solution. This force can be reduced by the presence of ϵ-aminocaproic acid.

An increased blood Lp(a)[1] level is associated with an increased risk for coronary and carotid artery disease (*1*, *2*). Studying the structure and assembly of Lp(a) is important for understanding its role in the formation of vessel wall diseases and in designing strategies for manipulating the turnover rate of the protein in plasma. Lp(a) is both atherogenic and thrombogenic, consisting of apo(a), apolipoprotein B (apoB), and a lipid core, with apo(a) linked to apoB by a disulfide bond and apoB bound to the lipid core noncovalently forming LDL (Figure 1; *3*). Apo(a), a glycopolypeptide, ranges in size from 300 to 800 kDa (MW) among different individuals. ApoB, a lysine-rich protein, has a molecular mass of 512 kDa. Because of the large molecular masses of Lp(a) and apo(a), both X-rays and nuclear magnetic resonance (NMR) are incapable of providing high-resolution images of the molecule. Electron microscopy (EM) by several groups over the past decade shows Lp(a) as individual spherical particles, with no apparent structural differences with respect to LDL (*4*).

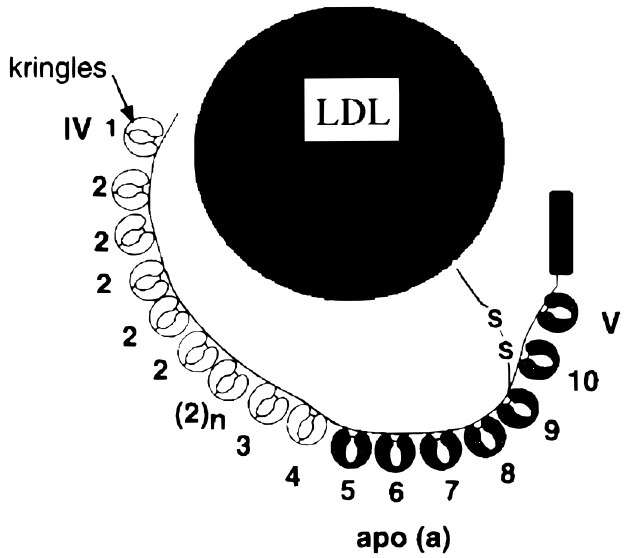

FIGURE 1: Schematic diagram of the structure of Lp(a). Apo(a) is covalently linked to LDL through a disulfide bond. Noncovalent interaction exists between apo(a) and LDL, especially the amino-terminal region of apo(a). Apo(a) consists of kringles similar to those in plasminogen and a protease domain at the carboxyl terminal. LDL consists of phospholipids and cholesterols wrapped with apoB. Apo(a) and apoB are linked with a disulfide bond.

Biochemical studies on Lp(a) assembly using recombinant apo(a) suggest that one end, namely, the carboxyl terminal, of apo(a) is responsible for apo(a) binding to the LDL particle (*5*, *6*). SFM imaging, for the first time, reveals Lp(a) as a spherical particle linked with a belt-like structure, with both ends of the belt attached to the sphere.

† The work was funded in part by U.S. Public Health Service Grant R37 HL 21788 (M. F. Arnsdorf) and a development grant from the Department of Medicine, University of Chicago and by the University of Chicago-Argonne National Laboratory Collaborative Grant Programs.

* Address for correspondence: Department of Medicine, University of Chicago, MC6080, 5841 S. Maryland Ave., Chicago, IL 60637. Phone: (773) 702-1086. Fax: (773) 702-8875. E-mail: shxu@medicine.bsd.uchicago.edu.

[1] Abbreviations: apo(a), apolipoprotein(a); apoB, apolipoprotein B; CNBr, cyanogen bromide; DTE, dithioerythritol; EACA, ϵ-aminocaproic acid; EDTA, ethylenediaminetetraacetic acid; EM, electron microscopy; GCS, glass coverslip; KI, kallikrein inactivator; LDL, low-density lipoprotein; Lp(a), lipoprotein A; MW, molecular mass; NMR, nuclear magnetic resonance; PMSF, phenylmethanesulfonyl fluoride; SFM, scanning (atomic) force microscopy; Si_3N_4, silicon nitride.

S0006-2960(97)02966-8 CCC: $15.00
Published on Web 06/06/1998

Apo(a) consists of multicopy units of so-called kringles, with each kringle having 80−85 amino acids and a COOH-terminal domain homologous to the trypsin-like serine protease (*7*). The number of kringles varies for different apo(a)s, which, in turn, results in different biological properties, including the atherothrombogenic potential of Lp(a) (*2*). The kringles in apo(a) are both structurally and functionally similar to the kringles in plasminogen and are responsible for interactions of Lp(a) with fibrinogen and fibrin, due in part to binding to the lysine residue in the substrate (*3*). X-ray crystallography of kringle 4 from plasminogen, homologous to kringles found in apo(a), reveals the key amino acid residues involved in the formation of a lysine-binding pocket (*8*, *9*). EM images of a truncated apo(a) mutant, which contains 17 of the kringles IV, reveal the molecules to be like chained balls with a resolution that is insufficient for distinguishing kringles interacting with each other (*10*). EM imaging of the apo(a) isolated from plasma Lp(a) has not been performed successfully because reduction of Lp(a), a step required for separation of apo(a) from LDL, leads to apo(a) aggregation.

Gel filtration studies of the reduced Lp(a) at various salt concentrations revealed that apo(a) and apoB are not separable except in the presence of 6 M guanidine hydrochloride or 50 mM EACA (*10*, *11*). Hydrodynamic modeling also suggests that apo(a) interacts with LDL through, at most, a few kringles, with the remainder of the molecule extending into solution (*10*). Besides the disulfide bond, strong noncovalent forces hold the Lp(a) molecule together. The bulk of apo(a) is extended away from the lipoprotein surface, where it may interact with other ligands (*10*).

Lipoprotein aggregation has been proposed for the formation of extracellular lipid deposition in normal and atherosclerotic human arterial intima. The lipoproteins aggregate and then fuse with each other in the extracellular space to form microscopically evident lipid deposits (*12*−*14*). Structures resembling lipoprotein aggregates have been visualized in human arterial intima by EM (*15*). Lp(a) aggregation has also been reported but has not been studied intensively. Little is known about the structure and properties of Lp(a) aggregates.

Understanding the forces of interaction among proteins, drug molecules, and other ligands is of great interest to both basic and clinical scientists (*16*, *17*). Determining and then manipulating these forces will contribute to a better understanding of the fundamental chemistry and physics of such interactions (*18*) and may have practical importance, for example, in the design of better and more efficient drugs (*17*, *19*).

Few attempts to study the forces between interacting biomolecules have been performed because of the lack of appropriate tools. The optical tweezer is limited to weak molecular interactions and is not appropriate for ligand and protein interactions (*20*, *21*). Magnetic force experiments (*22*), surface force apparatus (*23*), and pipet suction experiments (*24*) do not have high spatial resolution.

An SFM image results from interaction between the SFM tip and the sample (*25*, *26*). SFM can provide information regarding the surface structure and the surface properties of the specimen (*27*, *28*). The surface is the site where most biochemical reactions take place, such as substrate binding to proteins and enzymes as well as ligand binding to receptors. A variety of biological applications of SFM have been developed, which include nanometer resolution imaging of gap junctions (*29*, *30*), bacterial toxins (*31*), bacterial outer membrane proteins and channels (*32*, *33*), and DNA molecules (*34*, *35*); monitoring of biochemical processes (*36*); measurement of intermolecular interaction forces (*37*, *38*); and mapping of surface charges on a nanometer scale (*27*, *39*).

In chromatography techniques, one changes the ionic strength to influence the electrostatic interaction, the concentration of the chaotropic agent to influence the hydrophobic interaction or hydrogen bonds and the mechanical force between the ligand and the receptor (key and lock model), and the concentration of agonists and antagonists to compete for the ligand pocket. It is rather difficult and time-consuming to use conventional biochemical methods to determine quantitatively factors such as the effect of continuous change of ionic strength on apo(a) and its ligand, lysine. Both qualitative and quantitative analysis of the forces of interaction between apo(a) and lysine are critical to our understanding of the structure of the pocket for ligand binding and the dynamics of the binding process.

A new method for covalently coupling proteins onto the SFM tip has been developed (see Materials and Methods). This method allows the attachment of proteins or molecules with primary or secondary amines to the SFM tip. It allows the study of intermolecular interactions between proteins attached to the tip and ligands linked to the substrate. The analysis of the force of interaction by functionalized SFM allows quantitation of these interactions, and more importantly, these measurements are carried out at or near the level of single molecules instead of at the level of a population of molecules as is the case in common biochemical methods.

MATERIALS AND METHODS

Lp(a) Preparation. Lp(a) was isolated by sequential ultracentrifugation and lysine−Sepharose chromatography as described by Fless et al. (*40*). Protease inhibitors were added to plasma to prevent lipoprotein degradation (0.01% NaN_3, 0.15% EDTA, 10 000 units of KI/L, and 1 mM PMSF).

Apo(a) Preparation. Apo(a) was isolated from Lp(a) essentially as described by Edelstein et al. (*41*) and was stored in a 125 mM trehalose solution at −80 °C. Briefly, Lp(a) was incubated in a DTT solution for 10 min under argon gas at room temperature [1 mg/mL, 2 mM DTE, 10 mM sodium phosphate, 1 mM EDTA, and 0.02% NaN_3 (pH 7.5)] to reduce the disulfide bond between LDL and apo(a). EACA was then added to the reaction mixture (final concentration of 100 mM), and the solution was rotated slowly (7 rpm) in the dark at room temperature for 60 min. The reaction mixture was then dialyzed against phosphate buffer purged with N_2 gas [10 mM sodium phosphate, 1 mM EDTA, 0.02% NaN_3, and 100 mM EACA (pH 7.5)]. Then, an equal volume of 60% sucrose dissolved in the dialyzing buffer was mixed in, and the sample was ultracentrifuged at 412160*g* at room temperature for 18 h (TLA100.3 titanium rotor). The bottom 1 mL fraction, which contained apo(a), was then collected and analyzed for concentration and purity. The Lp(a), LDL, and apo(a) used were kindly provided by A. M. Scanu and C. Edelstein.

Imaging. A NanoScope III AFM-1 instrument was used in these experiments. The details of SFM operation have been published (for reviews, see refs *42* and *43*). Briefly, the SFM scanning tip is integrated into the end of a Si_3N_4 cantilever, and the cantilever deflects as the tip scans over the surface features (*25*). For the NanoScope III instrument used here, the deflection of the cantilever is detected optically by reflection of a laser beam off the cantilever and sensing of the amount of the reflected light beam with a two-element photodiode (*44*). A feedback system keeps the interaction force between the tip and the sample constant, i.e., the amount of deflection of the cantilever (height mode), by moving of the sample up and down with respect to the tip. The same piezoelectric scanner also moves the sample in the *x* and *y* directions. These three coordinates are used to create a three-dimensional image. The instrument is routinely calibrated with mica to ensure accurate movement in the $x-y$ plane.

Imaging generally begins in a 5×5 nm^2 area. When stable images are obtained, the scanning force is minimized by reduction of the set point voltage, and the scanning area is increased to the desired size. The raw data are plane-fit. The particle diameter and height are measured with the NanoScope III off-line data analysis program by use of the section profile. Unless specified, images are obtained both in air and in solution.

Preparation of Gold Particles. Colloidal gold particles (2 μL, 1.5×10^{12} particles/mL, stored in water with 0.1% NaN_3) were diluted in Millipore-filtered water (18 μL), spread onto a freshly peeled mica surface, and air-dried and stored in a desiccator at room temperature overnight.

Selection of Cantilever Tips. Colloidal gold particles were imaged with various cantilever tips. Those tips generating round images of the gold particles with relatively small tip-induced broadening were used (*45*).

Calibration of the SFM Tip with Colloidal Gold Particles. The details of the calibration procedure have been published (*28*, *45*). Briefly, colloidal gold particles, with a diameter similar to that of the imaged molecules, were scanned with the tip both before and after imaging of the specimen. The sectional sizes of the gold particles at various image heights were analyzed, which allowed one to derive the sectional radii at these image heights. The sectional radius is the sum of the sectional radius of the tip and of the gold particle at each of the points on the particle touched by the tip. Thus, on the basis of the measured sectional sizes of the image of the gold particle, one can derive the sectional radius of the tip at any point near the tip apex. When an actual specimen image was analyzed, the tip sectional radius was subtracted from the apparent sectional radius of the specimen to yield the actual size.

Specimen Preparation for SFM Imaging in Air and in Solution. An aliquot of protein, sufficient to form a layer on mica (1 cm in diameter), was mixed into phosphate solution preloaded on mica [10 mM sodium phosphate and 100 mM NaCl (pH 7.0)]. The specimen was incubated at room temperature for 5 min for adsorption of the protein to the surface of the mica. For imaging in solution, the specimen was then directly mounted onto the sample stage and imaged. Phosphate buffer was used as the imaging solution. For dry imaging, the mica disk was soaked in a weighing boat (3 cm in diameter) filled with 5 mL of the phosphate solution for removal of unbound proteins. Mica was then taken out of the solution and washed with a few drops of Millipore water and dried in air for at least 3 h before being imaged.

Coupling of Apo(a) to the CNBr-Activated Si_3N_4 Tip. The chemistry for attaching apo(a) to the SFM tip is similar to that of attaching proteins to Sepharose beads used in affinity chromatography. Partial oxidation and the residual impurity of the Si_3N_4 tip yield chemically reactive groups on the surface, including SiOH and Si_2NH (*46*, *47*). Reaction of these chemical groups with CNBr formed imido cyclic carbonate, a cyanate intermediate which readily reacts with primary and secondary amines as in lysine, and basic amino acid residues as in proteins such as apo(a) (*48*). Apo(a) was covalently attached to the SFM tip. Si_3N_4 tips were incubated in CNBr solution (0.5 g/mL CNBr, dissolved in Millipore water) at room temperature overnight. Because of the toxicity of CNBr, the reaction was carried out in a hood. The activated tips were first rinsed with Millipore water and then incubated with apo(a) diluted in $NaHCO_3$ solution [0.01 mg/mL protein, 50 mM $NaHCO_3$, and 500 mM NaCl (pH 8.3)] for 1 h at room temperature or at 4 °C overnight. The apo(a)-coupled tip was then incubated in a NH_4Ac solution (50 mM at pH 8.3) for the same time for removal of excess amine-reactive sites. The apo(a) tip was then stored in phosphate buffer at 4 °C until it was used later on the same day [10 mM sodium phosphate, 0.2% NaN_3, 1 mM PMSF, and 500 mM NaCl (pH 7.4)]. The lysine-coated Si_3N_4 tip was prepared in the same way as the apo(a) tip, except that apo(a) was replaced by lysine [10 mM lysine, 50 mM $NaHCO_3$, and 500 mM NaCl (pH 8.3)] to react with the CNBr-activated tip.

Preparation of Lysine−GCS. Glass coverslips were activated by incubation in CNBr dissolved in water (0.5 g/mL) overnight. The lysine−GCS was prepared by incubation of CNBr-activated glass coverslips with lysine solution for 2 h [1 mM lysine, 10 mM NH_4Ac, and 50 mM $NaHCO_3$ (pH 8.3)].

Adhesion Force Measurement. The adhesion force between the apo(a) tip and the lysine−GCS was measured with NanoScope III instrument, using the Force Cal program for acquisition of force curves. An aliquot of 80 μL of phosphate buffer [10 mM sodium phosphate and 150 mM NaCl (pH 7.0)] was added to the substrate on the sample stage. The cantilever holder was then placed in position without an O-ring, and the buffer solution was held in position by surface tension. Because it took less than 5 min to finish collecting the force curves for each experimental condition, the effect of solvent evaporation on the force measurement was negligible. Under each condition, 20 force curves were collected and analyzed, and the adhesion force was identified as the force of interaction between apo(a) and lysine. Standard deviations are presented. The scan rate was kept constant at 2 Hz, the scan started at 300 nm, and the scan size 1400 nm for all of the force curves collected. Long, narrow-legged Si_3N_4 cantilever tips were used.

RESULTS

Imaging Lp(a). Lp(a), untreated, was imaged in air as shown in Figure 2a−c. At low imaging resolution, Lp(a) appeared as individual spherical particles. When the resolu-

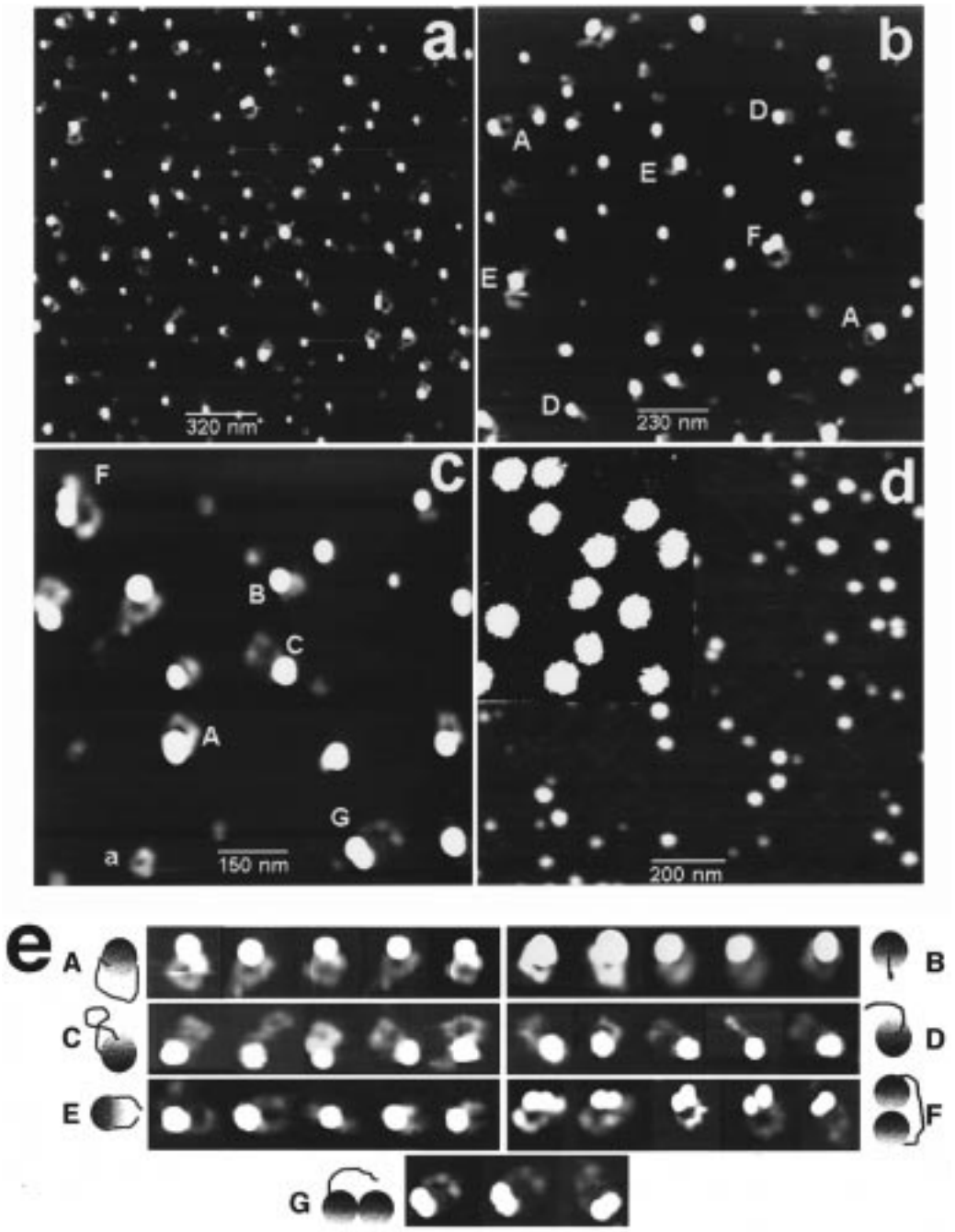

FIGURE 2: SFM imaging of Lp(a). Lp(a) was imaged in air (panels a−c), and the result was compared to that for LDL (panel d). Various shapes of Lp(a) were identified in SFM images, as schematically illustrated below the images (panel e). A belt-like structure was found with both of its ends attached to a sphere (shapes A−C in panels b, c, and e). Shapes A and B were believed to be different orientations of Lp(a)s. Shape C suggested that the belt could twist into a figure 8. Shapes D, E, and G seemed to be Lp(a)s with nicks at different spots on the belts. Shape F showed two spheres touching and linked by the belt. Shape G showed that a single belt was attached to one of two touching spheres. The LDL image showed none of the belt-like structures (panel d). Electron microscopy of Lp(a), as shown in the inset of panel d, failed to reveal the belt-like structure and showed no difference with respect to LDL images. Some apo(a) fragments were also found (a in panel c).

tion was increased, a belt-like structure appeared on the side of some of the spheres (Figure 2a−c); this was not observed for LDL under the same imaging conditions (Figure 2d). Seven characteristic structures (A−G) were identified and are illustrated in Figure 2. (A) A belt-like structure was attached to a sphere at two distant points, and a loop was formed, resulting in a large open hole in the middle. A repulsive force might exist between the center part of the belt and the LDL particle, which kept the center region away from the LDL surface. (B) A relatively short belt was closely attached to the sphere, and either a small hole or no hole was formed between the loop and the sphere; this could be a different orientation of configuration A caused by the various tilts of the plane of the apo(a) loop with respect to that of mica. If the plane of the apo(a) loop is parallel or nearly parallel to the surface of the mica, a large hole is then expected, as in the case of configuration A. On the other hand, if the plane of the loop is perpendicular or nearly perpendicular to the mica surface, then a small hole or no hole is expected, as in the case of configuration B. (C) The

belt, attached to the sphere at two sites, was twisted into a "figure 8". There are three possible reasons for the formation of the figure 8 shape. (1) The apo(a) belt is flexible. As the LDL sphere spins, the belt rotates at a different rate. (2) There is an interkringle interaction between two sequentially distant kringles. (3) Pretwisted apo(a) is assembled with LDL in vivo. (D) A belt was attached to the sphere with only one connection. I am not certain whether configuration D represents a dynamic state of the assembly of apo(a) with LDL or is a result of protease digestion or oxidation of the disulfide bond between apo(a) and apoB during purification and storage of the specimen (E in Figure 2b). Of course, I cannot rule out the possibility that shape D is also a regular configuration of Lp(a). (E) Two short belts were attached to the sphere at two distant sites. This configuration is likely to be the result of enzyme digestion of the apo(a) belt. The two belts attached to LDL in configuration E are too short to be two entire apo(a) molecules. In the image presented, none of the Lp(a) appeared with two full-length apo(a) belts. The identification of the E configuration also proves that two docking sites exist on LDL for the apo(a) molecule. The variation of the orientation of the two tails with respect to each other, as shown in Figure 2e, also supports the idea that the apo(a) belt is flexible. (F) A single belt was attached to each of two touching spheres, indicating the presence of an attractive force between LDL particles. Once the freedom of LDL particles is limited or the thermal energy is reduced, the LDL particles will bind to each other. The apo(a) belt in configuration F also varies in appearance, which is also believed to be a reflection of apo(a) flexibility. (G) A single belt was attached to one of two touching spheres. This configuration is the least frequently found among the seven different structural features. Like configuration D, it represents either a dynamic state of Lp(a) assembly or a protease digestion product of configuration F.

I cannot rule out the possibility that another belt is present for the two touching LDL spheres, but is not detected by SFM. I did not observe more than two LDL particles linked by a single belt. Shapes A, B, and E seemed to be more frequent than shapes C, D, F, and G. I am not certain whether one end of the belt is linked to the LDL particle only by a disulfide bond and the other by noncovalent protein−protein interactions. The fact that there is always a finite distance between the two docking points of the belt suggests that the interaction between apo(a) and LDL is specific. Some particles were probably apo(a) fragments (a in Figure 2c), which is an indication of contamination of protease in the Lp(a) sample. The presence of contaminated protease would explain the presence of configurations of Lp(a) like D, E, and G. Apo(a) belts in Lp(a) seem to form domains. As shown in configurations A, C, F, and G in Figure 2c and D, F, and G in Figure 2e, three domains seem to exist in the belts.

Quantitative Analysis of Lp(a) and LDL Images. Quantitative analysis of Lp(a) images showed the height of the LDL portion of Lp(a) to be 17.7 ± 0.39 nm ($n = 46$), the apparent diameter to be 45.2 ± 8.7 nm, and the calibrated diameter to be 24.8 ± 8.7 nm [calibrated according to the method we have previously described (*28*, *45*)]. The height, measured as 17.7 nm, which is similar to that from the SFM study of LDL (*49*), is smaller than the calibrated diameter and is also smaller than the 24.2 ± 4.2 nm reported from EM images (*4*). An ∼27% compression apparently occurred. The length of the belts attached to the sphere was measured to be 173.5 ± 6.6 nm ($n = 15$). The SFM tip, calibrated with 20 nm colloidal gold particles, was found to have a curvature radius of 65.3 ± 1.0 nm and a semivertical angle of 54.4 ± 0.5°.

Imaging of Apo(a). I also imaged apo(a)s isolated to study their high-order structure and to compare their differences with respect to those on Lp(a)s. The isolated apo(a)s appear as individual belts which are more stretched and thinner than those on Lp(a)s (Figure 3a−c vs Figure 2a−c). There are a few differences between these apo(a)s: (1) The presumed apo(a)s on Lp(a) images are attached either to the LDL particles or to fragments of apo(a)s; (2) the isolated apo(a)s are purified by treatment of Lp(a) with reducing agents; (3) lipids may be present in the apo(a) attached to LDL, but not in the isolated apo(a); and (4) the isolated apo(a)s rest flat on mica, whereas those on Lp(a)s are attached to the spheres and appear taller in SFM images, which would result in more SFM tip-induced convolution and cause the apo(a) to appear wider (*45*).

Apo(a)s isolated from Lp(a)s tend to crowd together, as shown in Figure 3b,c, an observation also reported by Phillips et al., who used EM for imaging (*10*). What causes this phenomenon is unknown, although interkringle interaction and the physical length of the molecules which makes them become tangled together are the possible explanations. How to dissociate these apo(a)s will be an issue for imaging of monomeric apo(a) molecules.

Apo(a) also forms an aggregated structure (Figure 3c,d). Of all of the proteins that I have imaged, apo(a) is the first to show a fishnet-like structure. None of the globular proteins that I have imaged, including earthworm hemoglobin, lysozymes, RNase, SUP35, nicotinic acetylcholine receptors, and colloidal gold particles, have shown this kind of structure. The fishnet-like structure was found with apo(a) adsorbed both on mica and on glass and in both dry and wet imaging. Therefore, it is unlikely to be due to the substrate. Because I can almost identify individual apo(a) molecules linked together, and because I have seen this kind of feature of apo(a) more than 20 times, I do not believe that this unique structure is caused by an artifact of specimen preparation. The aggregation of apo(a) suggests that apo(a)s interact with each other. The fishnet-like morphology suggests that the interaction occurs through multiple sites, probably through multiple kringles between two apo(a) molecules. It would be interesting to know which are the specific kringles involved in the interaction.

Morphologic Structure of Lp(a) and LDL Aggregates. Aggregates were found for LDLs and Lp(a)s stored for more than 3 weeks at 4 °C under N_2 gas in SFM images. Lp(a) aggregates appeared as leaf-like sheets (Figure 4a−c). Individual spherical particles aggregated in two dimensions. Under experimental conditions, no large-scale Lp(a) fusion was found, but the boundaries between some of the Lp(a) particles were less clear than those of Lp(a), which suggests that partial fusion had started. The height of the spherical particles was measured to be between 20 and 35 nm, suggesting less compression, but more variation, than for the monomers shown in Figure 2.

The aggregation of LDL appeared to have fewer characteristics but more lipid fusion compared to that of Lp(a)

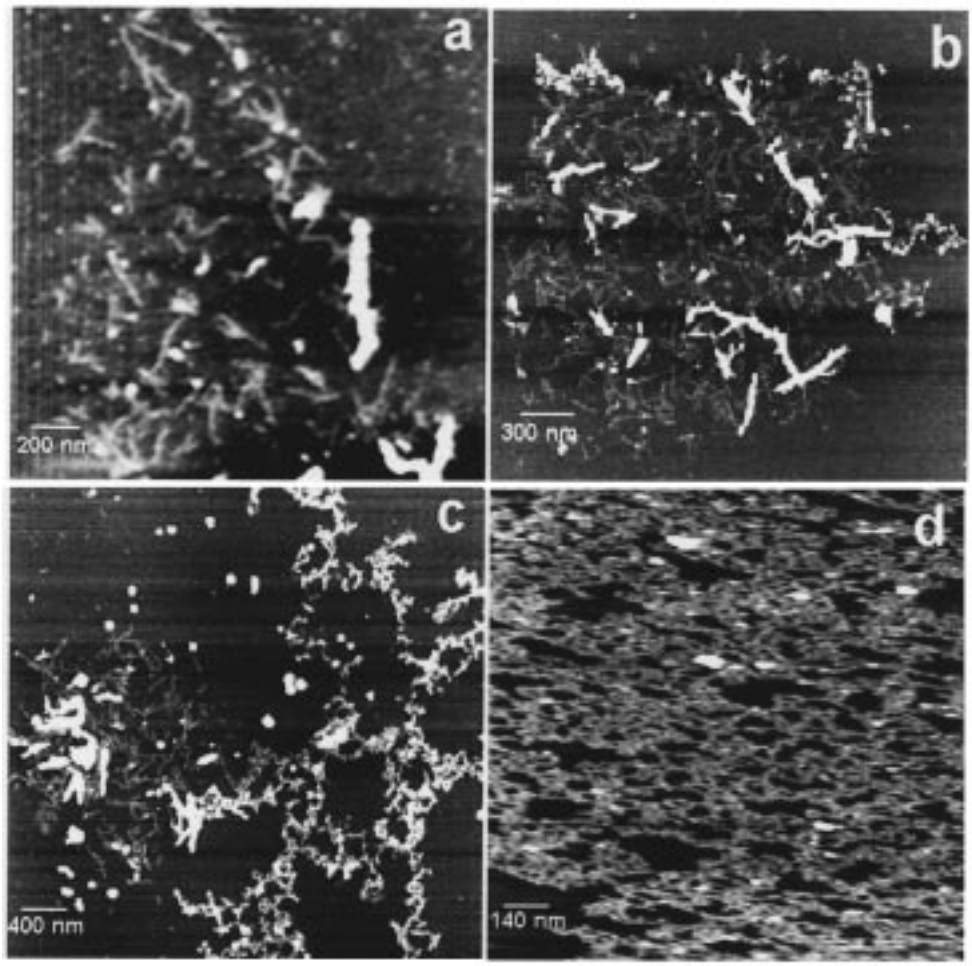

FIGURE 3: SFM images of apo(a) and its aggregates. Apo(a)s in trehalose, isolated from Lp(a) by the reduction method, were spread on mica and incubated for 2 min at room temperature [1 μg in 80 μL of 10 mM sodium phosphate buffer with 150 mM NaCl (pH 7.0)]. Unbound apo(a)s were removed by incubation of the specimen in 5 mL of phosphate buffer. For imaging in solution (panels a and d), an aliquot of 80 μL of the same phosphate buffer was applied to mica. For imaging in air (panels b and c), the mica disk was rinsed with a few drops of water and air-dried. Apo(a)s were found to be belt-like (panels a−c). These belt-like structures tend to crowd together, as shown in panels b and c. Aggregation of apo(a) was found to have fishnet-like morphology (panels c and d).

(Figure 4d). Both aggregates were more like a two-dimensional assembly, in contrast to prion formation in one-dimensional assembly (*50*, *51*). I do not know whether the assembly is induced by fusion of the lipids or by protein conformational change, although, in vivo, the presence of the heat shock proteins hsp 70 and hsp 60 in the lipid-rich core suggests the involvement of a protein conformational change (*52*, *53*). Apo(a) belts were not found in the aggregated Lp(a). The reason is unknown. The aggregates may possess multiple lysine-binding sites which can make the aggregates more competent than plasminogen for lysine-binding sites on fibrin and more efficient than individual Lp(a) monomers in binding to the extracellular matrix of human arterial intima and in blocking the hydrolysis of fibrin by plasmin.

Force of Interaction between Apo(a) and Its Ligands. Apo(a) was covalently bound to a standard Si_3N_4 cantilever tip, and lysine was covalently bound to Sepharose beads (lysine beads) which acted as a substrate. The sum of the force of interaction between the apo(a) tip and a lysine bead and the buoyant force of the bead (up to 150 μm in diameter) in solution [10 mM sodium phosphate and 100 mM NaCl (pH 7.4)] was found to be stronger than the sum of the gravity force and the force of interaction between the bead and glass. The apo(a) tip could drag the lysine bead and actually lift the bead from the surface of the glass. The bead remained bound to the apo(a) tip unless it was vigorously shaken (Figure 5). The lysine bead showed no binding to the lysozyme-coated tip or uncoated tip in the presence and absence of free apo(a) in the buffer. EACA competed for lysine-binding sites on apo(a). Addition of EACA [150 mM EACA, 10 mM sodium phosphate, and 500 mM NaCl (pH 7.4)] blocked the lysine bead binding to the apo(a) tip.

The density of the Sepharose bead is estimated to be between 1.02 and 1.1 g/mL (in Percoll Methodology and Applications, Pharmacia LKB Biotechnology, Piscataway, NJ). For a bead that is 100 μm diameter in water or in a low-concentration salt solution (less than 50 mM NaCl), the net force of gravity and buoyancy is between 1.25 and 6.28 nN. The force of interaction between a lysine−Sepharose bead and glass is measured to be about 0.5 nN; thus, the force needed to lift the bead from the glass is between 1.75 and 6.78 nN.

The Sepharose bead is porous, as shown in Figure 6, where the shadow or dark area represents a depression. Both the top view (left panel) and the surface plot (right panel) are presented here. The holes vary both in size and in shape, mostly with a length of about 1 μm and a width of $^1/_3$ to $^1/_2$

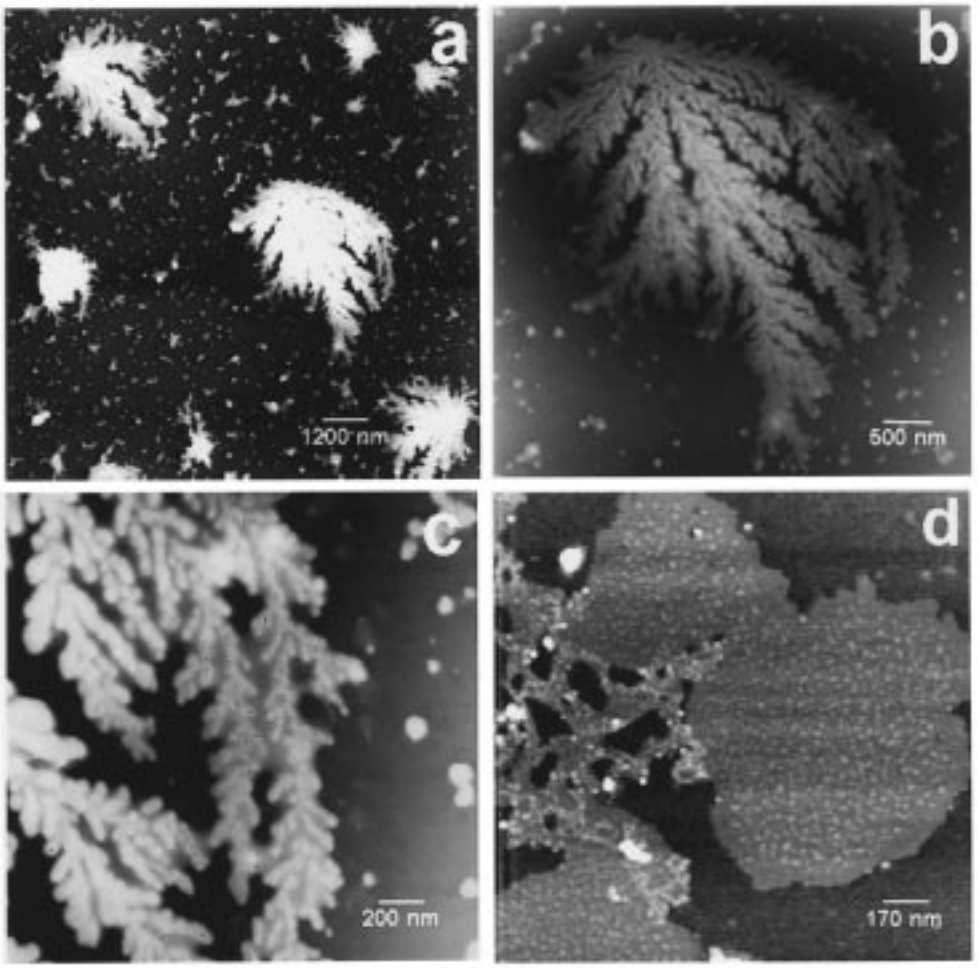

FIGURE 4: SFM images of Lp(a) and LDL aggregates. Aggregates were found for Lp(a)s and LDLs stored at 4 °C under N_2 for 3 weeks. Lipoproteins [0.1 μg in 80 μL of a 10 mM sodium phosphate solution with 100 mM NaCl (pH 7.0)] were spread on mica (1 cm in diameter) and incubated for 5 min. Unbound proteins were removed by incubation of the mica disk in the same phosphate buffer (5 mL). The mica disk was then rinsed with a few drops of water and air-dried for 3 h before being analyzed by SFM. The aggregates of Lp(a) were leaf-like (panels a−c) and were morphologically different from those of LDL (panel d). Panels a−c differ only in image magnification. Similar results were obtained when these lipoprotein aggregates were imaged in a phosphate solution.

μm. These large holes provide structural bases for the penetration of the SFM tip deep into the bead, which can result in a large contact area between them.

The force of interaction could be measured quantitatively between apo(a) and lysine when the lysine was attached covalently to a glass coverslip (lysine−GCS), which is heavier than a Sepharose bead. When the apo(a) tip was used for imaging of lysine−GCS, a force of interaction of 9 nN was observed, as compared to a force of less than 0.5 nN for an uncoated tip for imaging of lysine−GCS or a lysine-coated tip for imaging of plain glass (Figure 7). The 9 nN force is presumably required to rupture those interacting apo(a)−lysine pairs formed between the apo(a) tip and lysine−GCS.

The force of interaction between the apo(a) tip and lysine−GCS was found to be related to the salt concentration. A force recorded in 10 mM sodium phosphate buffer with 600 mM NaCl was 2−3-fold higher than that in the same buffer without NaCl. The addition of 150 mM EACA to the phosphate buffer lowered the force significantly to less than $^1/_2$ of the force measured in the phosphate buffer without NaCl and less than $^1/_5$ of that measured in phosphate buffer with NaCl. A relationship was found between the force of interaction and the NaCl concentration (Figure 7).

DISCUSSION

I have successfully imaged Lp(a) and identified the apo(a) portion attached with its two ends to the LDL sphere at two distant sites. Several other forms of Lp(a) isomers were also identified, namely, (1) one belt with its two ends bound to two touching spheres; (2) one belt with one end bound to one of the two touching spheres; (3) two shorter belts attached to one sphere, presumably a nick on the belt; (4) one belt attached to one sphere; and (5) one belt twisted into a figure 8 and attached to the sphere with its two ends. The Lp(a) images were calibrated with colloidal gold particles, and the calibrated size of the LDL portion of Lp(a) was 24.8 ± 8.7 nm, which is similar to the reported value based on EM analysis. The belts attached to the spheres in Lp(a) were measured for the first time for the entire apo(a) molecule to be about 173.5 ± 6.6 nm. The isolated apo(a)s are belt-like also and tend to crowd together. Lp(a), apo(a), and LDL form aggregates with different morphologies. Lp(a) aggregates are leaf-like, apo(a) aggregates fishnet-like, and LDL aggregates less characteristic two-dimensional irregular structures with more fusions. Apo(a) was successfully coated onto the SFM tip. The interaction force between the apo(a)-coated tip and the lysine−GCS was measured and found

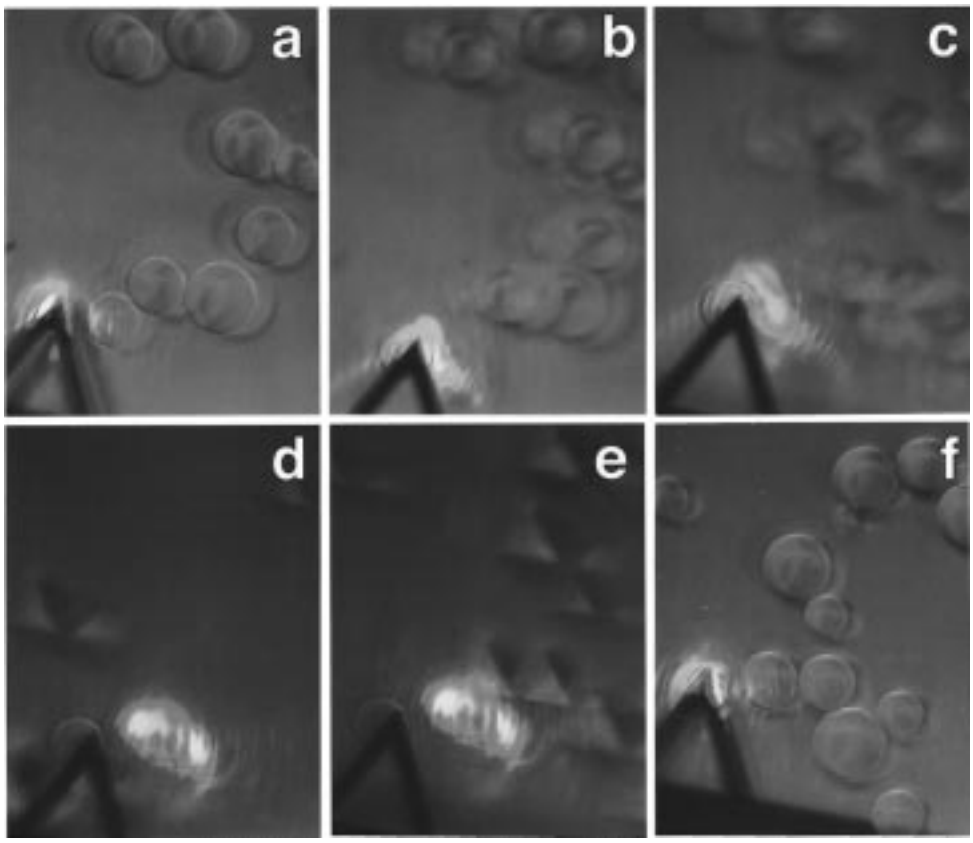

FIGURE 5: Lifting a lysine-coated bead with an apo(a)-coated tip. The apo(a)-coated tip was found to be able to lift a lysine-coated Sepharose 4B bead. The Sepharose 4B, with a density estimated to be between 1.02 and 1.1 g/mL, was slightly more dense than the medium. A Si_3N_4 tip coated with apo(a) by the CNBr method was allowed to touch a lysine-coated bead on a glass substrate in a phosphate solution [10 mM sodium phosphate and 150 mM NaCl (pH 7.0); panel a]. When the tip was raised, the lysine bead was found to be lifted up from the glass surface and removed laterally (panels b−e). Panel f shows that the same bead was placed back in its original spot. The presence of an excess amount of EACA (more than 600 mM) can block the binding of the lysine bead to the apo(a)-coated tip. The optical microscope was focused on the cantilever and beads (a and f) and the cantilever and the lifted bead (b−e).

to be related to the salt concentration of the bulk solution. The addition of EACA reduced the force 3-fold. This force is strong enough to lift a lysine-coated Sepharose bead and move the bead around. The lysine-coated Sepharose bead remained attached to the lysine tip unless the tip was vigorously shaken.

The two distant docking sites of apo(a) on LDL suggest that the kringles near the NH_2 and the COOH termini are involved in binding of apo(a) to LDL. The two short belts attached to LDL could be caused by Lp(a) degradation in vivo or could be caused by enzyme digestion during the isolation process, which generated a nick on the apo(a). Pancreatic elastase is known to be able to cut the apo(a) at six different sites (*54*).

It has been proposed, on the basis of some biochemical work, that Lp(a) assembly proceeds in two steps (*55*−*58*). First, apo(a) binds noncovalently to apoB-100, and the binding can be inhibited by lysine, proline, and hydroxylated proline or amino acid analogues such as EACA. Second, a disulfide bond is formed between the only free cysteine (residue 4057) in kringle IV9 (KIV9) of apo(a) and one of the free cysteines in apoB-100 (*59*). The presence of two docking sites of apo(a) on LDL is an indication of the presence of a noncovalent interaction, although it remains unclear which site binds to LDL first.

Assembly studies of Lp(a) using apo(a) deletion and substitution mutants reveal that (1) KIV6 and KIV7 are important for the first step of Lp(a) assembly, (2) Lp(a) assembly correlates strongly with the affinity of these constructs for lysine−Sepharose, and (3) increasing the absolute number of KIV repeats also contributes positively to the assembly (*6*). Specific kringles interacting with LDL are not identified by studying the deletion mutants. It is also not clear whether KIV6−KIV7 binds to LDL itself or affects the binding of other kringles. It is not clear what kringles of apo(a) are actually extended into the solution, why the second docking site of apo(a) is not detected by conventional biochemical methods, how many of the kringles between the two docking points are dispensable, and how the kringles interact with each other.

It is natural to question why EM failed to identify the belt-like structure in Lp(a) and, on the other hand, was able to image individual apo(a) molecules. Three explanations present themselves: (1) The apo(a)s attached to LDL are not as tall as LDL particles, and EM has trouble keeping both focused; (2) the belts are tilted toward the surface, or in other words, the plane of the belt is not parallel to the plane of the substrate surface and EM can focus on only a portion of the belt; and (3) the surface of the carbon films used in EM as the substrate for proteins is nonpolar, which is different from the negatively charged mica surface under aqueous solution. Lp(a)s absorbed on the surface of the carbon films can have orientations different from those on mica. SFM, based on an imaging principle totally different

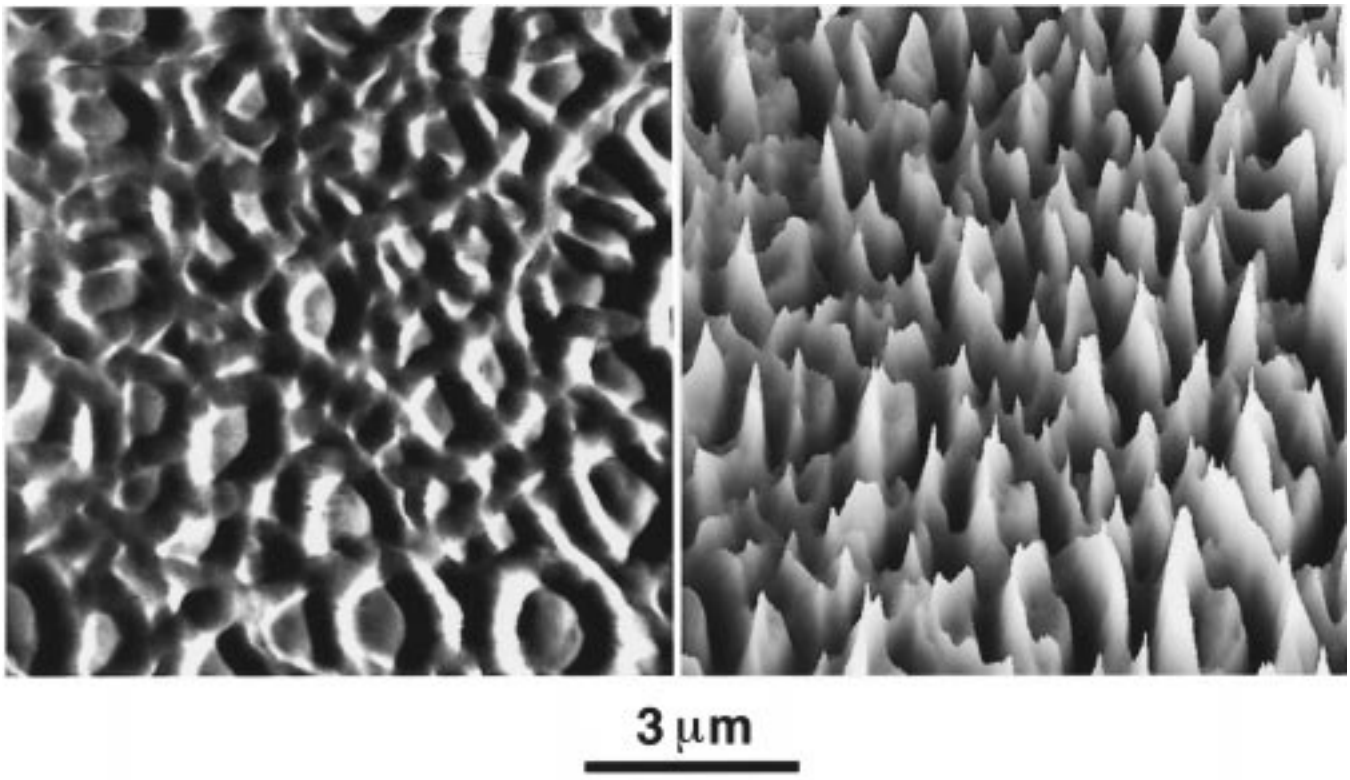

FIGURE 6: Image of the Sepharose bead. A layer of Sepharose 4Bs, with diameters between 45 and 160 μm, was placed on mica in phosphate buffer [10 mM sodium phosphate and 150 mM NaCl (pH 7.0)]. A portion of the Sepharose bead (9 μm × 9 μm) was then imaged as shown, with the height expressed in terms of brightness. The same image is displayed in both a top view (left) and a surface plot (right). Individual holes (the dark or shadowed area) can be identified in this porous mesh. The bright area is presumably the carbohydrate structure of the bead. The depressions vary in shape and size. Most depressions have a length of about 1 μm and a width of $^1/_3$ to $^1/_2$ μm.

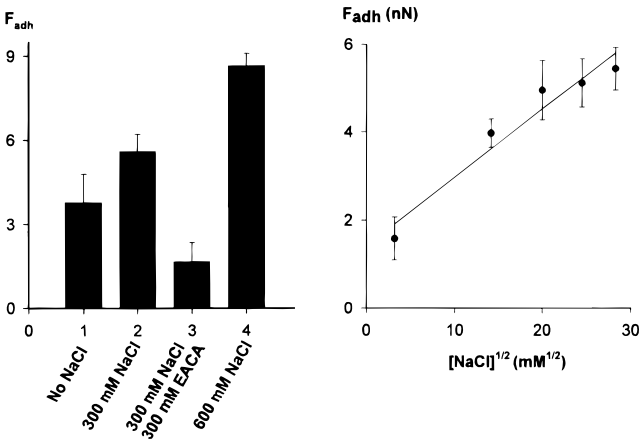

FIGURE 7: Force of interaction between the apo(a) tip and lysine−GCS. Glass coverslips, coated covalently with lysines by the CNBr method, were mounted onto the sample stage. An aliquot of 80 μL of testing buffer was applied to the glass coverslip. An apo(a)-coated tip clipped to the cantilever holder was then mounted on the sample stage. Force curves between the apo(a) tip and the lysine−GCS were then collected under various conditions (left, n = 20) in phosphate buffer (5 mM sodium phosphate at pH 7.0) and analyzed for the value of the adhesion forces. The experiments were repeated with three different tips. A large force was found at high ionic strength. EACA reduced the force. A linear relationship was found between the force and the square root of the concentration of NaCl (right).

from that of EM, is not affected by these putative problems. As a matter of fact, the tilt will make the portion of the apo(a) belt that is elevated from the substrate surface appear larger due to the tip convolution effect. Of course, the specimen treatment also differs between EM and SFM, which could affect the result.

Quantitative analysis of Lp(a) showed compression and tip-induced broadening of the protein. Compression and a tip-induced broadening effect are the two limitations associated with the SFM technique. I can minimize the compression by reducing the loading force or image the specimen with a tapping mode. The broadening effect can be calibrated by imaging of the colloidal gold particle.

Three kinds of interactions are potentially responsible for Lp(a) aggregation, namely, interactions between LDLs, between apo(a) and LDL, and/or between apo(a)s. LDL aggregates by themselves are shown in Figure 4. Much is known about the aggregation of LDL particles. Three factors are known to be able to induce LDL aggregation in vitro, namely, chemical oxidants (Cu^{2+}, H_2O_2, superoxide, and nitric oxide), biochemical incubation (phospholipase C, proteoglycans, heparin−gelatin−fibronectin, etc.), and mechanical processing (vortexing) (*15*). Interaction between apo(a) and LDL can also lead to Lp(a) aggregation. For the two LDL spheres linked by one apo(a) shown in Figure 2, there will be one more unoccupied docking site on each LDL sphere available for other apo(a)s to bind to. Each apo(a) molecule potentially can bind to two neighboring LDL spheres. Under appropriate conditions, it is possible, then, for the LDL spheres of Lp(a)s to be chained together by apo(a)s and form a giant Lp(a) aggregate. Interaction between apo(a)s can equally contribute or lead to Lp(a) aggregation. The aggregation of apo(a)s and the tendency of apo(a)s to crowd together as shown in Figure 3 are an indication of an interaction between different apo(a) molecules present. Apo(a) is longer than the diameter of the

LDL sphere. Sterically, the apo(a) part of Lp(a) has ample space to adapt itself to interacting with apo(a)s from other Lp(a) molecules and to bring the LDL spheres together, forming aggregates.

A tip with a radius of 65 nm would be able to carry up to 100 proteins on the edge of the tip, assuming that the arc of a twelfth sphere is considered the edge and that each apo(a) occupies an area of 100 nm^2 (*45*). The tip can reach as deep as 127 nm into a hole. The detectable depth of the depression varies mostly from 10 to 50 nm. The penetration of the SFM tip into the holes of Sepharose beads and the compressibility of the beads make the contact area between them larger than that between the apo(a) tip and the lysine−GCS. Therefore, more chemical bonds will be formed between the apo(a) tip and the lysine beads than between the apo(a) tip and the lysine−GCS.

The linear relationship between the adhesion force and the salt concentration shows a salt-induced shielding effect. In other words, some charges on the protein affect lysine binding to apo(a), and the electric screening of these charges is important for optimal binding of lysine to apo(a). Crystallographic study of the structure of the kringles 4 of plasminogen indicates that there are two tryptophan and aspartic acid residues and one phenylalanine, lysine, and arginine in or near the binding pocket for lysine. Mutations of any of these four charged amino acid residues cause the loss of the lysine-binding site (*60*). The charges around the binding pocket may fine-tune the orientation of the lysine residue in the pocket. The screening of the electric field by increasing the salt concentration of the bulk solution may then result in higher hydrophobic and stearic interactions between lysine and apo(a). The force measurement described above between the apo(a) tip and lysine−GCS also demonstrates that lysine attached to the Sepharose beads or GCS through a single covalent bond has enough flexibility to rotate and to adapt itself to the binding pocket in apo(a), as is demonstrated also in affinity chromatography for protein purification.

ACKNOWLEDGMENT

I thank Drs. Angelo M. Scanu, Celina Edelstein, and Duan P. Chen for helpful discussions. I thank Dr. Morton F. Arnsdorf, Mr. Hammad Ammer, and Mr. George Sawicki for their support of this work.

REFERENCES

1. Harpel, P. C., Hermann, A., Zhang, X., Ostfeld, I., and Borth, W. (1995) *Thromb. Haemostasis 74*, 382−386.
2. Wild, S. H., Fortmann, S. P., and Marcovina, S. M. (1997) *Arterioscler., Thromb., Vasc. Biol. 17* (2), 239−245.
3. Scanu, A. M., and Edelstein, C. (1995) *Biochim. Biophys. Acta 1256*, 1−12.
4. Edelstein, C., Italia, J. A., Klezovitch, O., and Scanu, A. M. (1996) *J. Lipid Res. 37*, 1786−1801.
5. Gabel, B. R., May, L. F., Marcovina, S. M., and Koschinsky, M. L. (1996) *Arterioscler., Thromb., Vasc. Biol. 16*, 1559−1567.
6. Frank, S., and Kostner, G. M. (1997) *Protein Eng. 10*, 291−298.
7. Mclean, J. W., Tomlinson, J. E., Kuang, W., Eaton, D. L., Chen, E. Y., Fless, G. M., Scanu, A. M., and Lawn, R. M. (1987) *Nature 320*, 132−137.
8. Wu, T. P., Padmanabhan, K., Tulinsky, A., and Mulichak, A. M. (1991) *Biochemistry 30*, 10589−10594.
9. Mulichak, A. M., Tulinsky, A., and Ravichandran, K. G. (1991) *Biochemistry 30*, 10576−10588.
10. Phillips, M. L., Lembertas, A. V., Schumaker, V. N., Lawn, R. M., Shire, S. J., and Zioncheck, T. F. (1993) *Biochemistry 32*, 3722−3728.
11. Fless, G. M., ZumMallen, M. E., and Scanu, A. M. (1985) *J. Lipid Res. 26*, 1224−1229.
12. Camejo, G. (1982) *Adv. Lipid Res. 19*, 1−53.
13. Frank, J. S., and Fogelman, A. M. (1989) *J. Lipid Res. 30*, 967−978.
14. Guyton, J. R., and Klemp, K. F. (1996) *Arteriocler., Thromb., Vasc. Biol. 16*, 4−11.
15. Guyton, J. R., and Klemp, K. F. (1993) *Am. J. Pathol. 143*, 1444−1457.
16. Fields, S., and Song, O. (1989) *Nature 340*, 245−246.
17. Frank, R. (1995) *J. Biotechnol. 41*, 259−272.
18. Leckband, D. E., Israelachvili, J. N., Schmitt, F. J., and Knoll, W. (1992) *Science 255*, 1419−1422.
19. Moran, E. J., Wilson, T. E., Cho, C. Y., Chorng, S. R., and Schultz, P. G. (1995) *Biopolymers 37*, 213−219.
20. Ashkin, A., Dziedzic, J. M., and Yamane, T. (1987) *Nature 330*, 769−771.
21. Kuo, S. C., and Sheetz, M. P. (1993) *Science 260*, 232−234.
22. Smith, S. B., Finzi, L., and Bustamante, C. (1992) *Science 258*, 1122−1126.
23. Israelachvili, J. (1994) in *Intermolecular and Surface Forces*, Chapters 3 and 6, Academic Press, San Diego.
24. Evans, E., Berk, D., and Leung, A. (1991) *Biophys. J. 59*, 849−860.
25. Binnig, G., Quate, C. F., and Gerber, C. (1986) *Phys. Rev. Lett. 56*, 930−933.
26. Hansma, P. K., Elings, V. B., Marti, O., and Bracker, C. E. (1988) *Science 242*, 209−216.
27. Xu, S., and Arnsdorf, M. F. (1995) *Proc. Natl. Acad. Sci. U.S.A. 92*, 10384−10388.
28. Xu, S., and Arnsdorf, M. F. (1997) *J. Microsc. (Oxford) 187*, 43−53.
29. Hoh, J., Lal, R., John, S. A., Revel, J.-P., and Arnsdorf, M. F. (1991) *Science 253*, 1405−1408.
30. Lal, R., John, S. A., and Arnsdorf, M. F. (1995) *Am. J. Physiol. 268*, C968−C977.
31. Yang, J., Mou, J., and Shao, Z. (1994) *FEBS Lett. 338*, 89−92.
32. Schabert, F. A., and Engel, A. (1994) *Biophys. J. 67*, 2394−2403.
33. Schabert, F. A., Henn, C., and Engel, A. (1995) *Science 268*, 92−94.
34. Bustamante, C., Vesenka, J., Tang, C. L., Rees, W., Authold, M., and Keller, R. (1992) *Biochemistry 31*, 22−26.
35. Hansma, H. G., Lanely, D. E., Bezanilla, M., Sinsheimer, R. L., and Hansma, P. K. (1995) *Biophys. J. 68*, 1672−1677.
36. Henderson, E., Hayelon, P., and Sakaguchi, D. (1992) *Science 257*, 1944−1946.
37. Florin, E. L., Moy, V. T., and Gaub, H. E. (1994) *Science 264*, 415−417.
38. Lee, G. U., Kidwell, D. A., and Colton, R. J. (1994) *Langmuir 10*, 354−357.
39. Frisbie, C. D., Rozsnyai, L. F., Noy, A., Wrighton, M. S., and Lieber, C. M. (1994) *Science 265*, 2071−2704.
40. Fless, G. M., Snyder, M. L., Furbee, J. W. J., Garcia-Hedo, M. T., and Mora, R. (1994) *Biochemistry 33*, 13492−13501.
41. Edelstein, C., Mandala, M., Pfaffinger, D., and Scanu, A. M. (1995) *Biochemistry 34*, 16483−16492.
42. Rugar, D., and Hansma, P. (1991) *Phys. Today 43*, 23−30.
43. Arnsdorf, M. F., and Xu, S. (1996) *J. Cardiovasc. Electrophysiol. 7*, 639−652.
44. Alexander, S., Hellemans, L., Martin, O., Schneir, J., Elings, V., and Hansma, P. K. (1989) *J. Appl. Phys. 65*, 164−167.
45. Xu, S., and Arnsdorf, M. F. (1994) *J. Microsc. (Oxford) 173*, 199−210.
46. Bergstrom, L., and Bostedt, E. (1990) *Colloids Surf. 49*, 183−197.
47. Senden, T. J., Drummond, C. J., and Kekicheff, P. (1994) *Langmuir 10*, 358−362.

48. Weetall, H. H. (1993) *Applied Biochem. Biotechnol. 41*, 157−188.
49. Yang, J., Mao, J., Yuan. J.-Y., and Shao, Z. (1996) *J. Microsoc. (Oxford) 182* (2), 106−113.
50. Jarrett, J. T., and Lansbury, P. T., Jr. (1993) *Cell 73*, 1055−1058.
51. Glover, J. R., Kowal, A. S., Schirmer, E. C., Patino, M. M., Liu, J., and Lindquist, S. (1997) *Cell 88*, 811−819.
52. Johnson, A. D., Berberian, P. A., Tytell, M., and Bond, M. G. (1995) *Arterioscler., Thromb., Vasc. Biol. 15*, 27−36.
53. Wick, G., Kleindienst, R., Schett, G., Amberger, A., and Xu, Q. (1995) *Int. Arch. Allergy Immunol. 107*, 130−131.
54. Edelstein, C., Italia, J. A., and Scanu, A. M. (1997) *J. Biol. Chem. 272*, 11079−11087.
55. Brunner, C., Kraft, H. G., Utermann, G., and Muller, H. L. (1993) *Proc. Natl. Acad. Sci. U.S.A. 90*, 11643−11647.
56. Koschinsky, M. L., Cote, G. P., Gabel, B., and van der Hoek, Y. Y. (1993) *J. Biol. Chem. 268*, 19819−19825.
57. Frank, S., Durovic, S., and Kostner, G. M. (1994) *Biochem. J. 304*, 27−30.
58. Frank, S., Durovic, S., Kostner, K., and Kostner, G. M. (1995) *Arterioscler., Thromb., Vasc. Biol. 15*, 1774−1780.
59. McCormick, S. P., Ng, J. K., Taylor, S., Flynn, L. M., Hammer, R. E., and Young, S. G. (1995) *Proc. Natl. Acad. Sci. U.S.A. 92*, 10147−10151.
60. Rouy, D., Koschinsky, M. L., Fleury, V., Chapman, J., and Angles-Cano, E. (1992) *Biochemistry 31*, 6333−6339.

BI9729662